https://doi.org/10.5194/essd-2022-279
Preprint. Discussion started: 17 August 2022

Open Access Earth System Science Data Discussions

Valgarður: A Database of the Petrophysical, Mineralogical, and Chemical Properties of Icelandic Rocks

Samuel W. Scott[1,2], Léa Lévy[3,4], Cari Covell[1], Hjalti Franzson[3], Benoit Gibert[5], Ágúst Valfells[1], Juliet Newson[1], Julia Frolova[6], Egill Júlíusson[7], María Sigríður Guðjónsdóttir[1]

[1]Department of Engineering, Reykjavik University, Reykjavik, 101, Iceland
[2]Institute of Earth Sciences, University of Iceland, Reykjavik, 101, Iceland
[3]Iceland Geosurvey, Reykjavik, 101, Iceland
[4]Faculty of Engineering, Lund University, Lund, 223 63, Sweden
[5]Department of Geosciences, University of Montpellier, Montpellier, 34095, France
[6]Faculty of Geology, Lomonosov Moscow State University, Moscow, Russia
[7]Landsvirkjun, Reykjavik, 103, Iceland

Correspondence to: Samuel Scott (samuelwarrenscott@gmail.com)

Abstract. The *Valgarður* database is a compilation of data describing the physical and geochemical properties of Icelandic rocks. The dataset comprises 1072 samples obtained from fossil and active geothermal systems, as well as relatively fresh volcanic rocks erupted in sub-aerial or sub-aqueous environments. The database includes petrophysical properties (effective and total porosity, grain density, permeability, electrical resistivity, acoustic velocities), as well as mineralogical and geochemical data obtained by point-counting, X-ray Fluorescence (XRF), quantitative X-ray Diffraction (XRD), and Cation Exchange Capacity (CEC) analyses. The motivation behind this database is threefold: (i) aid in the interpretation of geophysical data including uncertainty estimations, (ii) facilitate the parameterization of numerical reservoir models, and (iii) improve our understanding of the relationship between rock type, hydrothermal alteration and petrophysical properties.

1 Introduction

The physical properties of igneous and volcanic rocks exert a first-order control on a wide range of geological processes. Rock properties such as porosity and permeability reflect magmatic degassing, eruptive conditions, and environmental conditions related to tectonics, alteration, exhumation and weathering (Petford, 2003; Ceryan et al., 2008; Pola et al., 2012, 2014; Schön, 2015; Colombier et al., 2017; Villeneuve et al., 2019). Variability in the distribution of pore space, fractures, and minerals strongly influences the susceptibility of rock to undergo hydrothermal alteration, which can produce strong changes in mechanical and physical properties (Browne, 1978; Thompson, 1997; Saripalli et al., 2001; Dobson et al., 2003; Cox, 2005; Franzson et al., 2008; Frolova et al., 2014; Wyering et al., 2014; Sanchez-Alfaro et al., 2016; Heap et al., 2017; Mordensky et al., 2018; Cant et al., 2018; Navelot et al., 2018; Heap et al., 2020; Nicolas et al., 2020; Heap et al., 2022). Due to the natural heterogeneity in rock properties, constraining the quantitative relationships between different petrophysical properties and

https://doi.org/10.5194/essd-2022-279
Preprint. Discussion started: 17 August 2022

inferring the underlying causes of variability may require extensive petrophysical and mineralogical databases amenable to statistical analysis (Aladejare and Wang, 2017; Weydt et al., 2018; Bär et al., 2019; Asem and Gardoni, 2021).

Basalt is the most common rock type exposed on the surface of the Earth if the area of the ocean floor is included. Owing to the high reactivity of basaltic rocks during surface weathering and water-rock interaction (Wolff-Boenisch et al., 2006), basalt plays a major role in the global carbon cycle (Dessert et al., 2003). Accordingly, basaltic rocks are the main target rocks for carbon sequestration efforts involving natural mineral carbonation (Snæbjörnsdóttir et al., 2020). However, compared to sedimentary rocks, which constitute the major source rocks for fossil fuels, and granitic rocks, which comprise the majority of the continental crust, the petrophysical properties of basaltic rocks are less well-characterized (Heap and Violay, 2021).

Iceland, which is dominantly composed of basalt because of its location astride the Mid-Atlantic Ridge, hosts a large number (>30) of active volcanic systems and associated geothermal systems (Arnórsson, 1995). With continued spreading of the mid-ocean ridge, volcanic systems migrate out of the zone of active volcanism and undergo exhumation and erosion (Walker, 1963; Böðvarsson and Walker, 1964; Pálmason, 1980), exposing altered rocks and intrusive heat sources of so-called 'fossil' geothermal systems at the surface (Friðleifsson, 1983, 1984; Burchardt and Gudmundsson, 2009; Liotta et al., 2020).

Iceland's geology has been intensively studied. However, publicly-accessible datasets that provide petrophysical, geochemical, and petrographic data for a given sample set and additionally describe field relations are rare. Studies performed by Orkustofnun (the National Energy Authority) and Iceland Geosurvey (ÍSOR) between 1970-2010 resulted in an extensive dataset consisting of approximately 500 samples analyzed for total and effective porosity, permeability, chemical composition, and petrographic characteristics, which was first released in the *Valgarður*[1] database (Orkustofnun, 2018). This dataset has been useful in elucidating the interrelationship between porosity and permeability (Sigurdsson and Stefansson, 1994; Sigurdsson et al., 2000; Stefansson et al., 1997) and the relationship of these physical properties to the degree of hydrothermal alteration (Gudmundsson et al., 1995; Franzson et al., 2007). Here, we introduce an updated and expanded version of the database. The goal of this contribution is to ensure that this data remains accessible to future generations of geoscientists and reservoir engineers. In addition to helping constrain numerical models and geophysical inversions, this data can be used to better understand the interrelationship between lithology, hydrothermal alteration, and petrophysics.

[1]The database is named after Dr, Valgarður Stefánsson (1939-2006), a physicist, who was at the forefront of geothermal exploration in Iceland throughout his career at Orkustofnun. His main geothermal research objective was to define geothermal systems in terms of reservoir characteristics. Recognizing that a relative lack of petrophysical data hampered reliable reservoir modelling, he instigated and headed a comprehensive petrophysical research project to further reservoir modelling by combining petrophysics, geology, alteration and geochemistry. The rock samples used for this research were largely taken at various erosional levels of the Icelandic crust. Just over half of this database is derived from this work.

https://doi.org/10.5194/essd-2022-279
Preprint. Discussion started: 17 August 2022

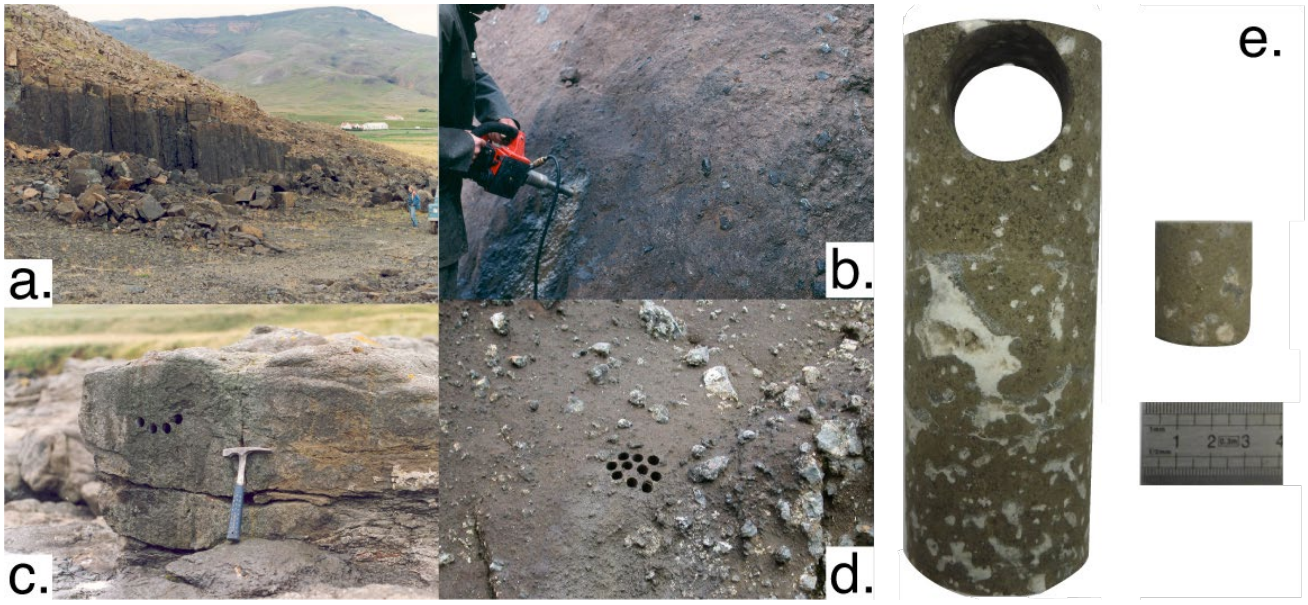

Figure 1. Photographs of sample collection. a. Basaltic intrusion (dolerite) located on in a quarry on the coast of Hvalfjörður (samples H-90 and H-91), b. Hyaloclastite tuff, located in Námagill (sample G-24), c. Basaltic lava flow, located in Kúludalsá to the south of Akrafjall (sample H-72), d. Hyaloclastite tuff breccia, showing embedded pillow basalt fragments (sample 170803-09). e. Spot core drilled into larger core obtained from 131 m depth in a borehole KH-1 in Krafla (sample L22). The rock is a lava flow altered to smectite-zeolite facies, with vesicles filled mainly with quartz, zeolites and calcite.

2 Structure and Contents of the Database

Valgarður is a publicly accessible database containing petrophysical and chemical/mineralogical analyses of Icelandic rocks. Although many studies have investigated the effect of elevated temperature and pressure on the petrophysical properties of Icelandic rocks (e.g. Vinciguerra et al., 2005; Jaya et al., 2010; Kristínsdóttir et al., 2010; Milsch et al., 2010; Adelinet et al., 2010; Adelinet et al., 2013; Grab et al., 2015; Eggertsson et al., 2020a,b; Nono et al., 2020; Kummerow et al., 2020; Weaver et al., 2020), at present we restrict the database to measurements at near-ambient conditions, in order to facilitate comparison between the different studies and ensure consistency among the reported data.

Sample collection involves drilling a ~2.5 cm diameter plug of variable length into a surface outcrop or section of core (Figure 1). Variability in the sample collection process and analytical methods is to be expected given the long period over which the underlying data comprising the database were collected. During assembly of the database, we sought to ensure that the results of the different studies are reported in a consistent manner. As different studies used different methods to analyze given petrophysical properties, each data point is accompanied by a description of the methodology or origin of the data.

Table 1 shows a description of the sources of the data for the database. The original 529 samples collected by Orkustofnun and Iceland Geosurvey (ÍSOR) between 1990-2010 that made up the first release of the Valgardur database mainly originate from hand-drilled cores taken at the surface within the neovolcanic zone or at erosional surfaces in the older strata at various

https://doi.org/10.5194/essd-2022-279
Preprint. Discussion started: 17 August 2022

Open Access Earth System Science Data Discussions

Table 1. Description of sources of data comprising the Valgarður database.

References	Description	Number of samples
Pálsson (1972); Pálsson et al., (1984); Friðleifsson (1973, 1975, 1978)	Early studies of petrophysical properties (grain density, effective/total porosity). Mainly comprises samples obtained at surface or from shallow boreholes. Relatively little description of geology and alteration; samples are described as 'Unaltered' or 'Altered', rather than an alteration zone shown in Table 3.	339
Sigurðsson and Stefánsson (1994); Guðmundsson et al. (1995); Sigurðsson (1998a,b); Sigurðsson et al. (2000); Sigurðsson and Stefánsson (2002); Franzson et al. (1997); Franzson et al. (2001); Franzson et al. (2008)	First systematic studies of rock properties in fossil and active geothermal systems. Includes petrophysical (grain density, total/effective porosity, permeability) as well as geochemical and petrographic data.	351
Friðleifsson & Vilmundardóttir (1998)	Detailed study of a single lava flow in the Reykjavik area. Samples taken at different depth levels within lava flow to see variation in petrophysical properties. Includes grain density, total/effective porosity, permeability, whole rock geochemistry, and point counting.	85
Franzson & Tulinius (1999)	Borehole samples from ÖJ-1 (in Ölkelduháls in the Hengill area). Samples obtained from altered hyaloclastite tuff at ~800 m depth. Includes electrical properties as well as grain density, total/effective porosity, permeability, whole rock geochemistry, and point counting.	14
Frolova et al. (2005); Franzson et al. (2010); Frolova (2010); Franzson et al. (2011)	Hyaloclastite tuff mainly obtained from surface outcrops in southwest Iceland. Most samples show a low degree of alteration. Includes grain density, total/effective porosity, permeability, whole rock geochemistry, acoustic velocities, and mechanical properties.	101
Flóvenz et al. (2005)	Investigation of the effect of alteration on the electrical properties of geothermal reservoir rocks. Borehole samples obtained from Krafla, Hengill, and Reykjanes. Includes electrical acoustic properties as well as grain density and effective porosity.	12
Reinsch et al. (2016); Nono et al. (2020)	Study of rock properties in fossil and active geothermal systems. Includes grain density, effective porosity and permeability as well as electrical and acoustic properties	20
Lévy et al. (2018, 2019a, 2019b, 2020a, 2020b)	Krafla core samples from research wells KH-1, KH-3, KH-5, and KH-6. Includes effective porosity and grain density (triple weight), permeability, electrical properties, and acoustic velocities. Quantitative mineral characterization using XRD.	94

https://doi.org/10.5194/essd-2022-279
Preprint. Discussion started: 17 August 2022

Gilbert et al. (2020)	Samples obtained from IDDP-2 at ~3.6-4.6 km depth. Includes grain density and effective porosity (triple weight) as well as electrical conductivity and acoustic properties.	20
Present study	Borehole samples from well ÞR-07 in Theistareykir. Effective porosity, grain density (triple weight), electrical properties, and acoustic velocities. Quantitative mineral characterization using XRD.	31
Present study	Surface samples from the Austurhorn gabbro in SE Iceland. Effective porosity, grain density (triple weight), electrical properties, and acoustic velocities.	3

palaeo-depths and alteration stages (Sigurðsson and Stefánsson, 1994; Guðmundsson et al., 1995; Franzson et al., 2007; Friðleifsson & Vilmundardóttir, 1998; Franzson et al., 2011). In this release of the database, we added data from 302 samples collected by Orkustofnun between 1970-1980 (Pálsson, 1972; Pálsson et al., 1984), 161 samples from downhole cores obtained from active geothermal systems (Flovenz et al., 2005; Franzson & Tulinius, 1999; Bär et al., 2019; Lévy et al., 2018, 2019a, 2019b, 2020a, 2020b; Gilbert et al., 2020; Nono et al., 2020), as well as previously unpublished analyses from borehole samples from the Theistareykir geothermal area and surface samples from the Austurhorn gabbro.

To facilitate simple and user-friendly handling, the database is provided in 'flat' format (one row per sample) rather than 'stacked' format (one row per measurement). The database is divided into two worksheets:

1. Petrophysical properties
2. Mineralogical and geochemical properties
3. Photographs of sampling sites
4. Additional hyaloclastite data
5. Extended references

The first and primary table reports measurements of petrophysical properties, including porosity, grain density, permeability, electrical resistivity and sonic velocities performed at close to ambient conditions, generally room temperature and atmospheric pressure. This table provides lithologic characterization, including detailed sample descriptions in both Icelandic and English, and description of alteration zone. This table also reports detailed sample metadata including sample type (surface or borehole), date and location of sample collection.

The second table reports geochemical and mineralogical data. The data reported on this worksheet includes petrographic observations (point-counting on thin sections), bulk rock geochemical analyses derived from X-ray fluorescence (XRF) analyses, or quantitative mineralogical assessments using X-ray diffraction (XRD). Although many studies have investigated the geochemistry and petrology of Icelandic rocks (e.g. Sigmarsson and Steinthórsson, 2007; Sigmarsson et al., 2008) and much of the available data has been compiled into a publicly-accessible database (Harðardóttir et al., 2022), in order to restrict

https://doi.org/10.5194/essd-2022-279
Preprint. Discussion started: 17 August 2022

the scope of the database, we only provide geochemical and mineralogical data for samples that also have petrophysical properties given in the first table.

A third table lists the names of files which contain images of many of the sampling locations for studies. These photographs have been included with the database to facilitate future investigations in the area. The fourth worksheet lists additional measurements performed of a subset of hyaloclastite tuff samples (Frolova et al., 2005), which are not included in the main database due to different methodology, i.e., effective porosity measurement using air as the saturating fluid rather than He gas (see below). The extended references worksheet lists all the references referred to as primary or secondary references in the database

2.1 Sample ID and References

The order in which samples are presented in the database is approximately chronological, based on the date of the reference and the order of the sample numbers within the reference. The sample ID is equivalent to the reported sample ID in the primary reference. Primary references indicate where the data was first published and/or best-documented; secondary references are also given if the data was reported or used in further studies, or in the case of borehole samples, provide the core logs reported after the drilling of the well. References that are not cited in this text but are cited in one of these columns are described in the references worksheet provided in the Excel database.

2.2 Location Coordinates and Description

A description of the sampling location is available for all samples. The location description is provided in Icelandic or English and is reported according to a geographic feature (mountain, lake, stream, etc.) or village/town. In the case of core samples, the name of the geothermal field and well from which the sample is obtained is given. Precise location coordinates describing the location of the samples are generally only available for samples collected after ca. 1995. For samples without location coordinates given in the primary reference (Pálsson, 1972; Pálsson et al., 1984), an approximate sampling location was estimated based on the sample location description. Therefore, there is significant uncertainty (up to 0.5 km or more) in the location of samples collected before 1995. For many of the samples, photographs were taken which show in some detail the location and the geological features (Figure 1). These photographs are provided in a supplement to the database.

The latitude and longitude of the sampling point at the surface in decimal degrees is reported according to the reference system WGS84 as well as in ISNET93, the latter being widely used in Iceland. The elevation is also shown in meters above sea level (m a.s.l.) and was obtained using Google Elevation services when not provided in the primary reference. Borehole samples show the coordinates at the wellhead and an accompanying depth (in meters), which may be uncertain for some samples collected by Pálsson et al. (1972, 1984).

Figure 2 shows the locations of all obtained surface and borehole samples. There is a greater abundance of samples from the southwest of Iceland, including the area around Reykjavik, Akranes, Borganes, and the Reykjanes peninsula. Many of the samples are taken at deep erosional levels within fossil geothermal systems, including the Geitafell central volcano located in

https://doi.org/10.5194/essd-2022-279
Preprint. Discussion started: 17 August 2022

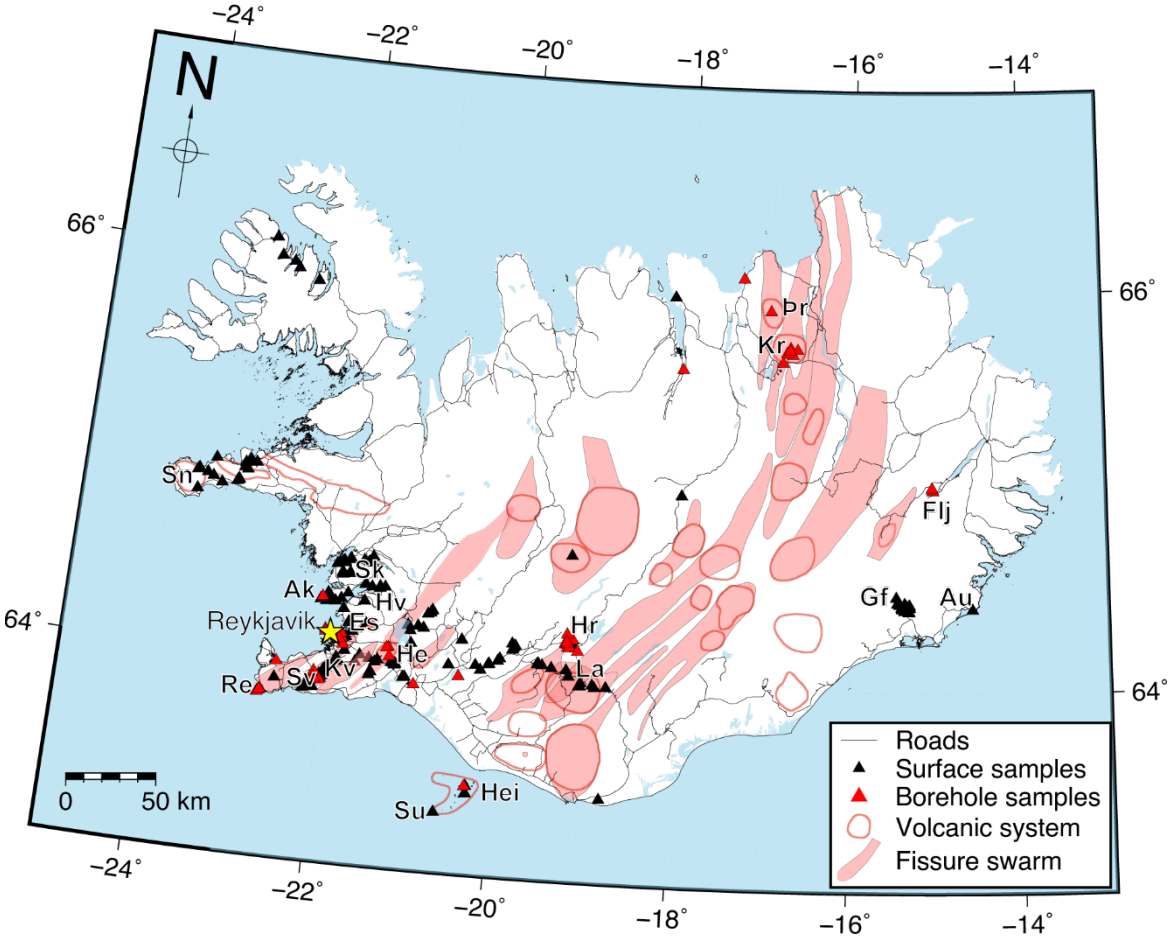

Figure 2. Map of Iceland showing the locations of surface (black triangles) and borehole samples (red triangles) comprising the database. Volcanic systems outlined with thick red lines and associated fissure swarms highlighted in light red. Roads are shown as thin black lines. Locations mentioned in text: Ak = Akranes, Au = Austurhorn, Es = Eja, Flj = Fljótsdalshreppur, Gf = Geitafell, He = Hengill, Hei = Heimaey, Hr = Hrauneyjar, Hv = Hvalfjörður, Kv = Krýsuvík, La = Landmannalaugar, Re = Reykjanes, Sk = Skarðsheiði, Sn = Snæfellsness, Su = Surtsey, Sv = Svartsengi, Þr = Theistareykir. Incorporates data from the Icelandic Institute of Natural History (IINH, 2022).

the Hornafjörður region in the southeast (Friðleifsson, 1983a,b; Friðleifsson, 1984), the Hafnarfjall-Skarðsheiði central volcano located in the west (Franzson, 1978), and the Esja volcanic region located close to Reykjavik (Friðleifsson, 1973). There are several surface samples of altered volcanic rocks collected from active geothermal areas, including the Reykjanes peninsula (Svartsengi, Krýsuvík, and Reykjanes), the Hengill region, and Landmannalaugar. Borehole samples are available from the major active geothermal areas (Hengill, Reykjanes, Krafla, and Theistareykir), as well as from several wells drilled outside of thermal areas during the evaluation of hydropower projects in Fljótsdalshreppur and Hrauneyjar (Pálsson et al., 1972, 1984).

https://doi.org/10.5194/essd-2022-279
Preprint. Discussion started: 17 August 2022

2.3 Rock type characterization

The sample description provides a summary of characteristics on the scale of the hand sample, including but not limited to grain size, color, vesicle size, the presence of layering, fractures, joints and fissures, and relevance to other samples. Sample descriptions that were originally provided only in Icelandic were translated into English and are listed in separate columns. The level of detail of sample description varies between the different studies. Each sample is assigned to one of eight broad lithological categories and 24 more detailed lithological identifiers, following the classification scheme of Guðmundsson et al. (1995) (Table 2). Lithological identifiers were determined based on the interpretation of the geological context and visual characteristics, rather than whole-rock chemical analyses. For borehole samples, the sample description is obtained from the description of the core log at the logged depth.

Table 2. List of lithological identifiers, detailed description of rock types covered by that identifier, and number of samples in the database corresponding to each lithology.

Broad lithological category	Lithological identifier	Number of samples
Lava flow	Flow-top breccia	34
	Fine-medium grained basaltic lava	222
	Medium-coarse grained basaltic lava	98
	Porphyritic basaltic lava	109
	Total	463
Hyaloclastite	Hyaloclastite breccia	77
	Hyaloclastite tuff	178
	Hyaloclastite sediment	12
	Total	267
Pillow basalt	Pillow basalt	41
Silicic volcanic	Rhyolite lava	13
	Rhyolite hyaloclastite	35
	Rhyolite tuff	10
	Rhyolite breccia	4
	Ignimbrite	7
	Total	69
Intermediate volcanic	Icelandite (andesite)	13
	Dacite	2
	Basaltic andesite	6

https://doi.org/10.5194/essd-2022-279
Preprint. Discussion started: 17 August 2022

	Total	21
Basaltic intrusion	Fine-medium grained basaltic intrusion	54
	Medium-coarse grained basaltic intrusion	53
	Porphyritic basaltic intrusion	16
	Gabbro	16
	Total	139
Silicic intrusion	Rhyolite dyke	17
	Granophyre	7
	Total	24
Intermediate intrusion	Diorite	6
Sediment		42

Among extrusive basaltic volcanic rocks, one key distinction is between lava flows, which are erupted sub-aerially, and hyaloclastites, which are erupted sub-glacially. Fresh, microcrystalline olivine basaltic lava flows are referred to as *grágrýti* in Icelandic. Tholeiitic lava flows, evolved from more basic olivine basalt, are often referred to as *blágrýti*. The latter usually show flow-banding. Porphyritic basalts show feldspar, olivine and pyroxene phenocrysts. Basaltic lava flows are often vesicular, especially towards the tops of the individual lava flow units, where they develop a thick surface rubble or a ropy texture. Such units are referred to as flow-top breccias (*kargi*) or entablature/cube-jointed basalt (*kubbaberg*), which often shows irregular columnar jointing.

Hyaloclastite formations often contain denser pillows or pillow fragments embedded in a tuff matrix (Figure 1d). Hyaloclastite (*móberg*) contains a higher proportion of glassy material compared to lava flows. Hyaloclastite breccias and pillow basalts show significant heterogeneity on the scale of cm-m. To maximize the homogeneity among the cores drilled for a given rock sample, hyaloclastite samples were obtained from the dominantly glass-rich tuff matrix (e.g Fig. 1d). Due to the strong contrast in the physical properties of the pillow basalt fragments compared to the tuffaceous matrix, pillow basalts comprise a separate category.

Silicic volcanic rocks are often found as 50-100 m thick flows in the vicinity of volcanic vents. Silicic volcanic products include vesicular glassy pyroclastics such as pumice, black, glassy obsidian, which forms from rapid cooling at the margins of rhyolitic lava flows, perlite, a glassy variety of rhyolite with high water content, and ignimbrite, which forms during explosive eruptions when volcanic material cascades down slope as ash flows. Intermediate volcanic rocks include icelandite (which is considered interchangeable for andesite) as well as dacite.

Among intrusive rock types, basaltic intrusions are distinguished from silicic or intermediate intrusions. Basaltic intrusions include both gabbro, which crystallizes in larger subsurface magma bodies, as well as dolerite (sometimes referred to as diabase), which is found in basaltic dykes, including cone-sheets. Silicic intrusions include both rhyolite dykes as well as

https://doi.org/10.5194/essd-2022-279
Preprint. Discussion started: 17 August 2022

granophyre, which usually shows fine-scale intergrowth of quartz and feldspar, as well as microgranite, which lacks granophyric intergrowths. Intermediate intrusive rocks including diorite are relatively rare. It should also be envisaged that intrusions may be of very variable age in relation to the geothermal system it intrudes.

Sedimentary rocks include clay-rich lacustrine sediments, glacial tillite, conglomerates, sandstone, as well as interbasaltic beds. Further distinction between these rock types is not made in the database due to the emphasis on volcanic and igneous rocks. It should though be noted that sedimentary grains are near exclusively of igneous origin.

In addition to the lithological classification, each sample is assigned to one of the main alteration zones identified in Icelandic rocks (Table 3). Most of alteration minerals in Iceland fall in the Ca^{2+} (stilbite-heulandite-laumontite-wairakite) and Ca^{2+}+Mg^{2+} (smectite-chlorite-epidote-actinolite) series of minerals (Walker, 1960; Walker, 1974; Kristmannsdóttir and Tómasson, 1978; Kristmannsdóttir, 1979; Lonker et al., 1993; Franzson and Gunnlaugsson, 2020; Escobedo et al., 2021). With increasing depth and temperature, these alteration zones are the smectite-zeolite zone, the mixed-layer clay zone, the chlorite-epidote zone, the epidote-actinolite zone, and the amphibole zone (Franzson et al., 2008). In some studies (Kristmannsdóttir 1979; Sveinbjörnsdóttir 1992), further distinction is made between a chlorite zone and the chlorite-epidote zone; for this study, we combine these two zones for simplicity and to facilitate comparison among the different studies. In addition, we combine the amphibole zone with the epidote-actinolite zone. Rocks without obvious alteration mineralogy are described as unaltered, although they may have undergone some extent of palagonitization.

Table 3. Description of alteration zones and number of samples in the database corresponding to each alteration zone.

Alteration zone	Description	Number of samples
Unaltered	Rocks without obvious alteration mineralogy. Many glass-rich hyaloclastite rocks have undergone some palagonitization but are still classified as unaltered (see text).	508
Smectite-zeolite	Replacement of basaltic glass and olivine by smectite clay (mostly saponite). Zeolite minerals precipitate in open vesicles but are also found dispersed in replaced glass. Occurs at temperatures below 200 ºC. Often coexists with chalcedony.	170
Mixed-layer clay	Interlaying of smectite and chlorite occurs to an increasing extent at 200-230 ºC. Onset of plagioclase alteration. In a more acidic environment, mixed-layer smectite-illite is observed but is rare.	88
Chlorite-epidote	Chlorite is the dominant sheet silicate at rock temperatures >230 ºC. Epidote occurs sporadically >240 ºC but may precipitate in larger quantities at high permeability. Often coexists with prehnite and wairakite.	159
Epidote-actinolite	High-grade greenschist facies assemblage. Actinolite forms in fine-grained aggregates together with chlorite and epidote at temperatures >280 ºC. May include secondary pyroxenes or feldspars (albite) at higher temperatures. The zone includes also wollastonite.	113

https://doi.org/10.5194/essd-2022-279
Preprint. Discussion started: 17 August 2022

Palagonitization occurs as post-eruptive process entailing the hydration of basaltic glass and replacement by secondary minerals, including zeolites and smectites (Stroncik and Schminke, 2002). Although this is a type of alteration process, it does not correspond to a specific alteration zone as observed in active and fossil geothermal systems. Note that variable porosity and permeability has a pronounced effect on the alteration intensity of the rock.

3 Data Acquisition

Measurements at ambient conditions of room temperature and atmospheric pressure include grain density, porosity, permeability, electrical conductivity, and acoustic velocities. Table 4 shows the number of samples with data corresponding to the different petrophysical and mineralogical properties. Only a few samples were analyzed for mechanical properties. Depending on the source of the data, different analytical techniques were used to measure a given petrophysical property. This can make it challenging to report the measured quantities in a consistent manner.

Table 4. Number of samples with both petrophysical/mineralogical data for different properties in the database.

	Effective porosity	Total porosity	Point-counting	Grain density	Air perm.	Brine perm.	Intrin. perm.	Elec. resist.	XRF	XRD
Effective porosity	1054	512	351	1047	499	102	496	176	340	124
Total porosity	512	513	157	513	129	36	127	9	191	0
Point-counting	351	157	359	353	287	41	285	10	287	0
Grain density	1047	513	353	1050	499	97	490	177	341	120
Air permeability	499	129	287	499	499	87	495	55	262	40
Brine permeability	102	36	41	97	87	102	86	51	45	45
Intrinsic permeability	496	127	285	490	495	86	496	55	259	41
Electrical resistivity	176	9	10	177	55	51	55	177	10	119
XRF	340	191	287	341	262	45	259	10	353	0
XRD	124	0	0	120	40	45	41	119	0	124

3.1 Porosity and Grain Density

Porosity is differentiated between effective porosity (the fraction of bulk volume occupied by interconnected pore space) and total porosity (the fraction of bulk volume occupied by pore space). In igneous and volcanic rocks, gas bubbles may form

https://doi.org/10.5194/essd-2022-279
Preprint. Discussion started: 17 August 2022

unconnected pores, particularly when volatile content is low, and porosity may be largely unconnected when porosity is less than ~0.1 (Colombier et al., 2017). Different analytical methods are available for quantifying porosity, among the most widely used methods are gas expansion (He pycnometry) and saturation/imbibition methods (Anovitz and Cole, 2015). While measurement of effective porosity using methods such as triple-weighting is non-destructive, determination of total porosity requires crushing the sample to measure the density of the solid material via conventional methods such as Hg displacement. Gas expansion methods are based on Boyle's law and the ideal gas law. A gas, usually He, due to its ability to penetrate narrow pore throats (>1 nm; Anovitz and Cole, 2015), expands isothermally from a reference cell at a known pressure into the sample container. The resulting equilibrium pressure reflects the volume of the pores into which the He gas has penetrated, calculated using Boyle's law. As the bulk volume of the sample V_{bulk} is known based on the geometry of the sample, effective porosity can be calculated following Eq. (1):

$$\phi_{eff} = \frac{V_{pore}}{V_{bulk}} \quad (1)$$

where V_{pore} is the fraction of interconnected pore space.

Saturation/imbibition methods are based on weighing a dry sample prior to full saturation with a wetting fluid (W_{dry}), after immersing the fluid in a saturating fluid for an extended period ($W_{immersed}$), and again after removing excess brine from the surface of the sample (W_{sat}). The porosity is then given by Eq. (2):

$$\phi_{eff} = \frac{V_{bulk} - V_{matrix}}{V_{bulk}} = \frac{V_{bulk} - (W_{dry} - (W_{immersed} - W_{crad}) + W_{crad})/\rho_{fluid}}{V_{bulk}} \quad (2)$$

where ρ_{fluid} is the density of the saturating fluid and W_{crad} is the weight of the cradle used to immerse the sample.

Effective porosities measured using gas expansion and triple weighing methods can yield similar results, at least within the margin of uncertainty of <2 %. This is demonstrated in Figure 3a, which reports effective porosity data collected by both methods on core samples from Krafla (Lévy et al., 2018, 2020b). For gas expansion measurements, an additional source of uncertainty is related to the choice of the saturating gas. Figure 3b compares effective porosity measurements performed on a set of hyaloclastite samples using either He (Franzson et al., 2011) or air (Frolova et al., 2005) as the saturating gas, and shows that effective porosity of samples measured using air is lower, likely due to the lesser ability of air to penetrate the microporosity. However, as these measurements were performed on different core plugs obtained from a given rock outcrop (e.g. Fig. 1d), this uncertainty may also reflect the natural heterogeneity in the sampled rock.

https://doi.org/10.5194/essd-2022-279
Preprint. Discussion started: 17 August 2022

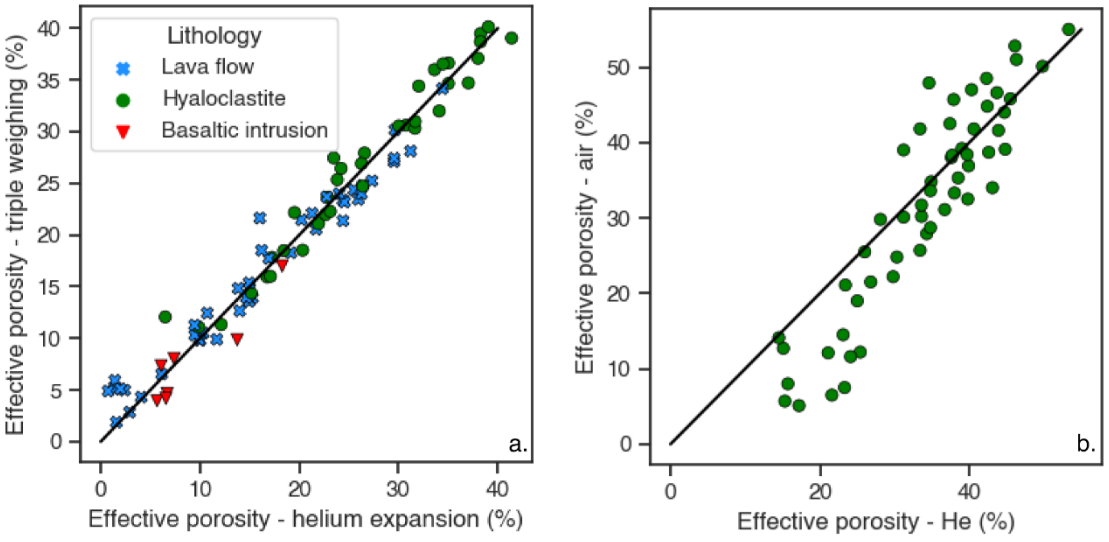

Figure 3. Comparison of effective porosity measurements using different measurement techniques. a. Effective porosity obtained by helium expansion and versus effective porosity measured using triple weighting. Data derived from a subset of core samples originating from Krafla (Lévy et al., 2018, 2020b). b. Comparison of effective porosity measurements on hyaloclastite tuffs using He or air as the saturating gas. Data is from Franzson et al. (2011).

All of the total porosity and most of the grain density data reported in this database were determined by pulverizing the sample and measuring the density of crushed materials using conventional techniques (e.g. Hg displacement). Total porosity can be calculated following Eq. (3):

$$\phi_{tot} = \frac{V_{bulk} - V_{grain}}{V_{bulk}} = \frac{\rho_{grain} - \rho_{bulk}}{\rho_{grain}} \quad (3)$$

As noted in Colombier et al. (2017), although accurate measurement of the density of the solid, pore-free phase(s) in the volcanic rock is required to calculate total porosity, heterogeneity in the phenocryst assemblage between clasts or variations in bulk composition may be common. Grain density can also be approximated based on effective porosity measurements from triple-weighting following Eq. (4):

$$\rho_{grain,TW} = \frac{W_{dry}}{V_{matrix}} = \frac{W_{dry}}{V_{bulk} - \frac{(W_{sat} - W_{dry})}{\rho_{fluid}}} \quad (4)$$

However, if there is a significant fraction of unconnected porosity, Eq. (4) will systematically overestimate grain density. However, Figure 4 shows that lava flows altered to smectite-zeolite facies alteration show similar distribution of grain density, whether measured by Hg displacement or triple-weighting (Fig. 4a). On the other hand, hyaloclastites altered to similar conditions show significantly larger average grain density, when measured by triple weighting (~2.75 g cm^{-3}) than by Hg displacement (~2.6 g cm^{-3}), as illustrated by Fig. 4b. Other factors might also explain this discrepancy, most notably that many of the samples analyzed using triple-weighting are core samples, while most of the samples analyzed using Hg displacement were derived from surface exposures.

https://doi.org/10.5194/essd-2022-279
Preprint. Discussion started: 17 August 2022

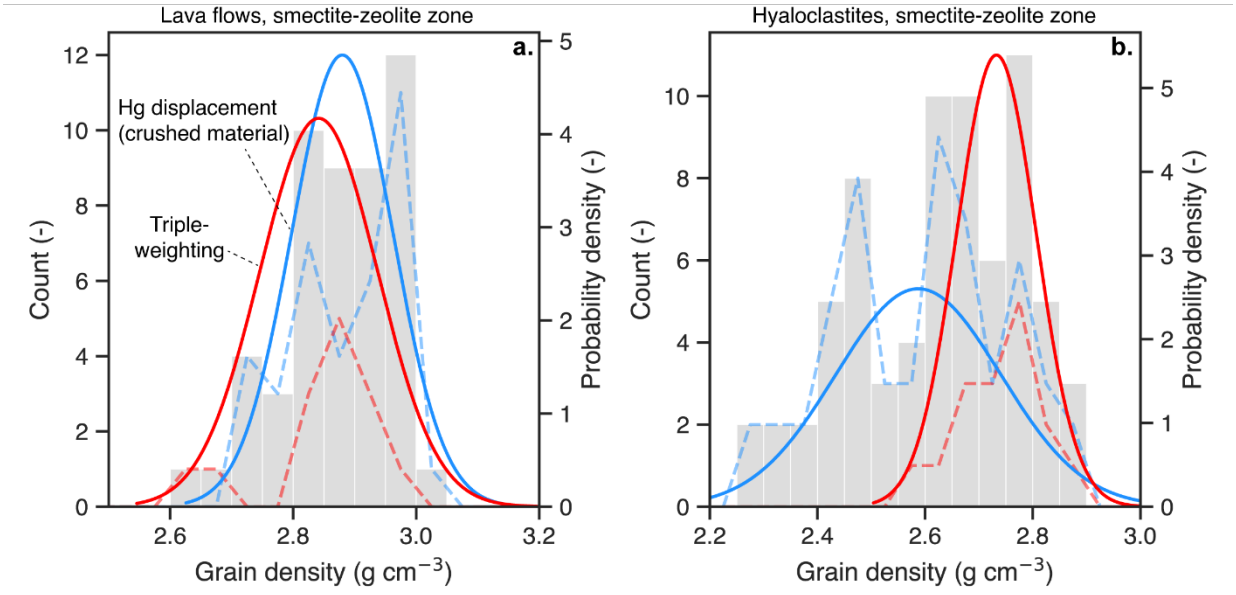

Figure 4. Grain density obtained by mercury displacement (blue dashed lines) and triple-weighting (red dashed lines) for (a) lava flows and (b) hyaloclastites. All data is shown in grey and a normal distribution fit to the data for each respective measurement technique is shown with solid blue or solid red lines. Note that all of the samples for which grain density was measured by triple-weighting were core samples, while most of the samples for which grain density was measured using Hg displacement were surface samples. This could also affect the difference seen in (b).

Porosity was also assessed in 352 samples by point counting. In this case, a thin section of the sample is prepared, a regular grid with a given number of points (usually 200 or 1000 points) was arrayed onto the thin section, and identification of mineralogy or pore space at each point was performed. Depending on the study, different levels of distinction were made between primary minerals, glass, pore space, and alteration minerals. While pore space represents remaining porosity, primary porosity includes both remaining porosity as well as alteration minerals that have precipitated into previously open vesicles. Several samples were measured by a combination of gas expansion methods and point counting, facilitating comparison of the obtained porosity values using the different methods. Generally, measured porosity by gas expansion or triple weighting is higher than that obtained by point counting.

3.2 Permeability

Permeability is measured at unsteady-state of flow of gas, usually helium or argon. Many of the early samples (Guðmundsson et al., 1995) were measured at Core Laboratories (formerly Western Atlas Core Laboratories) using the CMS-300 device, consisting of a gas cylinder with a known volume, a pressure sensor, and a core holder that can be opened into a gas cylinder charged with helium gas, generally up to 16.5 bar-gauge, and the atmosphere. Samples from Lévy et al. (2020) were measured at University of Montpellier, by a stationary method on cylindrical samples confined at a pressure of 40 bars. A constant argon

https://doi.org/10.5194/essd-2022-279
Preprint. Discussion started: 17 August 2022

pressure was imposed at the sample inlet and pressure at the sample outlet was maintained at 1 bar, and argon flow rate were measured by a gas flow-meter. For each sample, the argon pressure at the inlet were systematically varied from about 5 to 40 bars in order to evaluate the intrinsic permeability as described below.

Pressure in the gas cylinder is recorded as a function of time, and the pressure in and out of the core is known, and the flow through the core is proportional to the pressure drop. Darcy's law is then used to calculate permeability from the above quantities:

$$k = -\frac{q\mu}{A\left(\frac{dp}{dx}\right)} \quad (5)$$

where k is the rock permeability, q is the volumetric flow rate of the gas or liquid, μ is the viscosity of the fluid, A is the cross-sectional area, and $\frac{dp}{dx}$ quantifies the pressure drop along the core.

When using gas or liquid to measure permeability in rock samples, it is necessary to correct the measured permeability for systematic measurement error resulting from the sample geometry and the properties of the fluid (Klinkenberg, 1941). Thus, intrinsic permeability is calculated from measured gas permeability at a range of gas pressures using the Klinkenberg correction, which is based on the following equation:

$$k_i = \frac{k_g}{\left(1+\frac{b}{p_m}\right)} \quad (6)$$

where k_g is the measured gas permeability calculated from equation (5), p_m is the average gas pressure at which k_g is measured, and b is the Klinkenberg coefficient, taken as a constant for a certain gas and a certain rock. The Klinkenberg coefficient and intrinsic permeability k_i are obtained by plotting measured gas permeability at a range of pressures against $\frac{1}{p_m}$, with the slope corresponding to k_i and the y-intercept k_i (when p_m goes to infinity). The Klinkenberg coefficient depends on various properties of the rock, particularly the geometry of the pore space, and generally increases with decreasing permeability. As a result, relative measurement accuracy is greater (±5%) for high permeability rocks (≥10^{-14} m^2) and reaches up to ±400% in low permeability rocks (≤10^{-16} m^2) (Filomena et al., 2014). For samples from Lévy et al. (2019, 2020), only Klinkenberg-corrected permeability is available.

Measured permeabilities listed in the database range over six orders of magnitude, from ~10^{-18} m^2 (near the lower limit of many measurement techniques) to ~10^{-12} m^2. Figure 5a shows that air apparent permeability often exceeds brine apparent permeability, often by several orders of magnitude. Measurements with air permeability less than brine permeability are generally considered unreliable. Figure 5b shows the difference between the air apparent permeability and intrinsic permeability, showing that the magnitude of the Klinkenberg correction increases with decreasing permeability.

https://doi.org/10.5194/essd-2022-279
Preprint. Discussion started: 17 August 2022

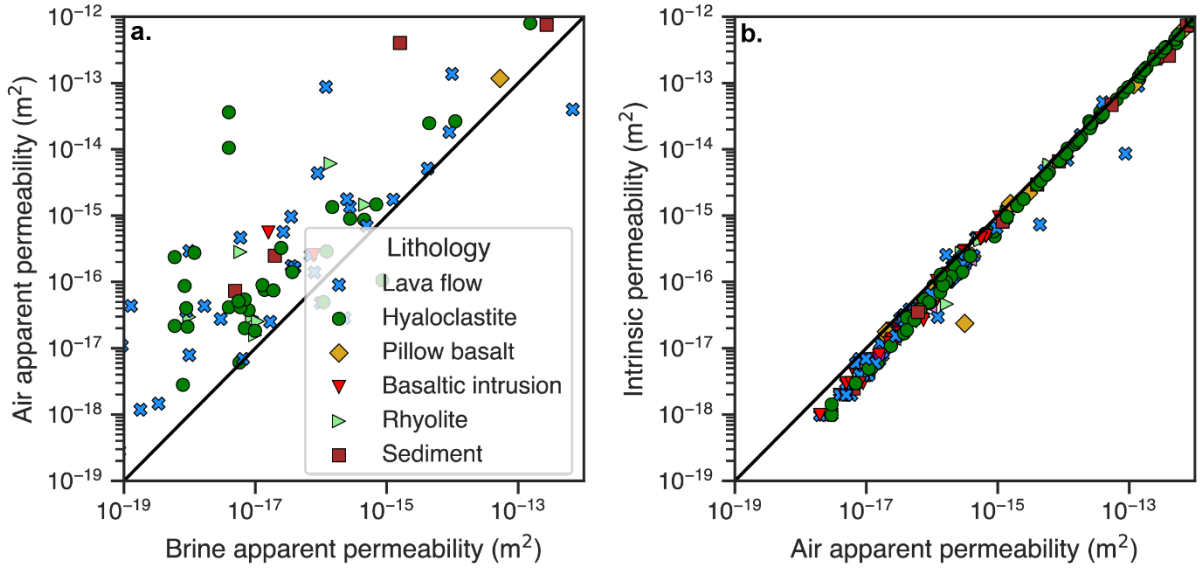

295 **Figure 5. Permeability data. a. Comparison of brine apparent permeability and air apparent permeability. b. Comparison of air apparent permeability and intrinsic permeability; the difference between these two quantities reflects the Klinkenberg correction (see text).**

3.3 Electrical Conductivity

Electrical conductivity (and its inverse, electrical resistivity) are intrinsic rock properties that measure how strong the material 300 resists electrical current, as given by Ohm's law, $R = \frac{U}{I}$, where R is resistance, U voltage, and I current. When an alternating current flows through a material, the electrical resistivity is characterized not only by the ratio of the magnitude of current and voltage, but also the difference in their phases, as expressed by the electrical impedance, a complex number written as a function of angular frequency ω and phase angle θ for sinusoidal current and voltage as:

$$Z(\omega) = \frac{U_o e^{i(\omega t+\theta_U)}}{I_o e^{i(\omega t+\theta_u)}} = |Z(\omega)|e^{i\theta(\omega)} = Z'(\omega) + iZ''(\omega) \quad (7)$$

305 where (U_o, θ_U) and (I_o, θ_I) are the amplitudes and phases of the sinusoidal voltage and current, respectively, t is time, and $\theta(\omega) = \theta_I - \theta_U$ is the frequency-dependent phase angle (generally negative, corresponding to a phase delay of voltage relative to current). For sample plugs with a given length L and cross-sectional area A, the electrical conductivity σ is related to Z by:

$$\sigma(\omega) = |\sigma(\omega)|e^{i\theta(\omega)} = \sigma' + i\sigma'' = \frac{Z'(\omega)}{|Z(\omega)|^2}\frac{L}{A} + \frac{Z''(\omega)}{|Z(\omega)|^2}\frac{L}{A} \quad (8)$$

310 where $|\sigma|$ and θ are the frequency-dependent modulus and phase angle of the complex conductivity, respectively, and σ' and σ'' are the in-phase (real) and quadrature (imaginary) parts of the complex conductivity, respectively.

https://doi.org/10.5194/essd-2022-279
Preprint. Discussion started: 17 August 2022

The complex conductivity is obtained by measuring the impedance spectrum of the sample over a frequency range (generally 0.1 to 10^6 Hz). Flovenz et al. (2005) used a Zahner IM-6 electrochemical workstation, while Lévy et al. (2018, 2019a, 2019b, 2020) used a Solartron 1260 impedance meter. Results show that there is a slight dependence of resistivity on measurement frequency, particularly above 10 Hz). Two types of sample-holders and configurations were used: 1) the two-electrode set-up, where the sample is sandwiched between two metallic electrodes acting as current and voltage electrodes, and 2) a four-electrode set-up (Vinegar & Waxman, 1984), where the voltage and current electrodes are separated. In the latter, metallic (Ni, Pt, Ag) electrodes are used to inject the current and non-polarizable Ag/AgCl electrodes are used for voltage measurement. Although the four-electrode set-up improves the quality of the conductivity spectra, especially below 10 kHz, the values obtained by both set-ups are comparable at 1 kHz, where effects of electrode polarization are negligible (Lévy et al., 2019b). In the *Valgarður* database, resistivity measurements (inverse of in-phase conductivity) at low-salinity and room temperature are presented; in addition, the frequency and experimental configuration (two- or four-electrode) are noted in the "Remarks" column next to each data point.

In rocks where free ions in pore water are the only charge carriers, the in-phase conductivity of a volume of rock σ_{bulk} is governed by Archie's law:

$$\sigma_{bulk} = \frac{\sigma_w}{F} \quad (9)$$

where σ_w is the conductivity of the pore fluid and F is the formation factor, representing the tortuosity of the current path. While F is related to the porosity, the relationship is more indeterminate in igneous rocks than in sedimentary rocks (see e.g. Lévy et al., 2018). In rocks containing clay minerals, an additional term influences the rock conductivity, and the simplest way of writing this additional term is given by Rink and Schopper (1974):

$$\sigma_{bulk} = \frac{\sigma_w}{F} + \sigma_s \quad (10)$$

where σ_s is the "surface" or "interface" conductivity, resulting from ion exchange with the solid matrix. More complex equations also describe the contribution from clay minerals (see e.g. Waxman and Smits, 1968 and Lévy et al., 2018) but this linear equation is often preferred. The formation factor and surface conductivity are typically determined by a series of conductivity measurements on the same sample saturated at different pore fluid salinities (conductivities). Uncertainty estimations for the formation factor can be found in Lévy et al. (2019b), including corresponding equations for this uncertainty calculation.

Figure 6 shows an example of how measurements of electrical conductivity vary as a function of the salinity of the saturating fluid and the initial smectite content of the rock. In Figure 6, sample L22 corresponds to a lava flow altered to smectite-zeolite facies alteration, and sample L48 to a lava flow altered to chlorite-epidote facies alteration. The higher smectite content in L22 results in a higher CEC (see below) compared to L48. A higher CEC corresponds to an increasing role of surface conduction, resulting from ion exchange reactions with clays. The larger formation factor in L22 is explained by the presence of smectite alteration minerals, which partially clog the original pore network and prevent the diffusion of free ions in the pore space by the fluid, but also allow efficient conduction of electrical charge along the smectite clays.

https://doi.org/10.5194/essd-2022-279
Preprint. Discussion started: 17 August 2022

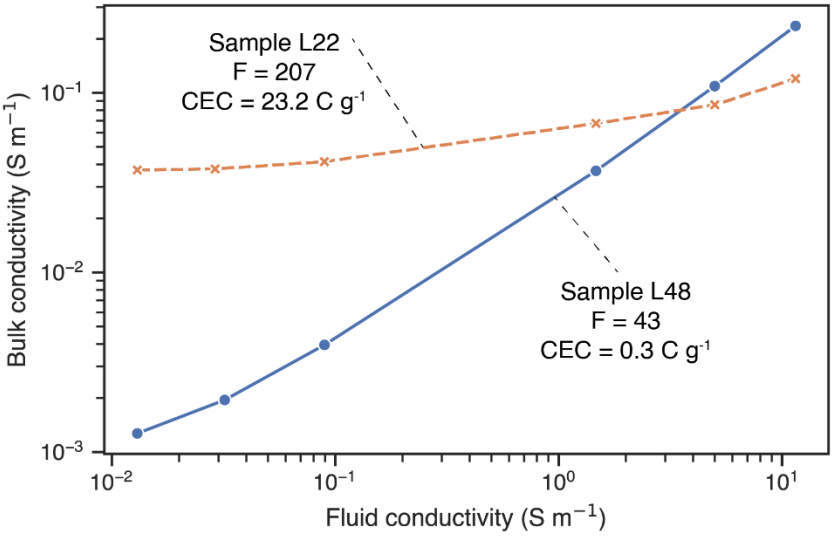

345

Figure 6. Results from electrical measurements at 1 kHz versus fluid conductivity for two samples from Lévy et al. (2018) with different electrical properties. The formation factor (F) and cation exchange capacity (CEC) for the two samples are noted.

At a given salinity, an apparent formation factor F_{app} can be determined by $\frac{1}{F_{app}} = \frac{\sigma_{bulk}}{\sigma_{fluid}}$. This value is reported for samples where resistivity was only measured at one fluid salinity (Franzson & Tulinius, 1999). It is equal or close to the true formation
350 factor if (i) there are no clay minerals or (ii) the pore space is saturated with high-salinity fluid (the contribution from free ions in the pore space largely dominates that of clay minerals). However, when resistivity measurements are carried out on samples that may contain clay minerals and have been saturated with only one fluid salinity, care should be taken when interpreting F_{app} because the contribution of surface conduction to the bulk conductivity may be significant (Fig. 6).

3.4 Petrographic and geochemical characterization

355 Four different methods are used to characterize the mineralogy and geochemistry of the samples: 1) Point-counting by petrographic observation, 2) X-Ray Fluorescence (XRF) on fine powders, 3) powder X-ray Diffraction (XRD) and 4) Cation Exchange Capacity (CEC). The former two methods were used exclusively on the samples analyzed by Orkustofnun and Iceland Geosurvey (Sigurðsson and Stefánsson, 1994; Guðmundsson et al., 1995; Franzson et al., 2008; Friðleifsson & Vilmundardóttir, 1998; Franzson & Tulinius, 1999; Franzson et al., 2011). The latter two methods were used to assess the
360 mineralogy in core samples from Lévy et al. (2018, 2019a, 2019b and 2020b).

Point counting was used to quantify primary porosity, i.e. the original open space in rock prior to alteration (dominantly vesicles and minor fractures), and to assess how much of that porosity had been filled by deposition of alteration minerals. Generally, two hundred points were counted on each rock thin section and grouped into the following categories: primary mineral, altered primary mineral, precipitate in vesicles, precipitate in fractures, intercrystalline pores, and unfilled fractures.

https://doi.org/10.5194/essd-2022-279
Preprint. Discussion started: 17 August 2022

365 A more detailed classification scheme was used in Friðleifsson & Vilmundardóttir (1998), with primary minerals separated by plagioclase, pyroxene, olivine, and opaque minerals. For the hyaloclastite samples investigated in Franzson et al. (2011), 1000 points were counted and grouped as one of the following: porosity, unaltered glass, altered glass, unaltered primary mineral, altered primary mineral, zeolite, clay, calcite or other.

Bulk rock chemical analyses were performed by two commercial chemical laboratories, The Caleb Brett Laboratory in England
370 and McGill University in Canada. Both used standard XRF techniques. Values for samples analyzed by both laboratories are generally within analytical error. The samples were analyzed for major, minor, and several trace elements (Zr, Y, Zn, Cu, Rb, Sr, Nb, Ga, Ce, V, Pb, U, Th and As). Major element analyses in the database are presented both in unnormalized form and after removing LOI (loss on ignition, see below) and renormalizing the composition to 100%. Figure 7a shows the samples categorized by lithology plotted on a total alkali – silica diagram. Note that this diagram shows both altered and unaltered
375 rocks. The vast majority of the samples plot in the basalt field, as expected. While it has been suggested that hydrothermal alteration in Icelandic rocks is close to an isochemical process (Franzson et al., 2008), the lava flows, hyaloclastites, and basaltic intrusions that plot outside of this field due to the effects of alteration, e.g. silicification in the upflow zones of geothermal systems. In addition, many of the silicic volcanic rocks or silicic intrusions are depleted in silica compared to what would be expected given the lithological classification based on geologic context and visual characteristics. One chemical

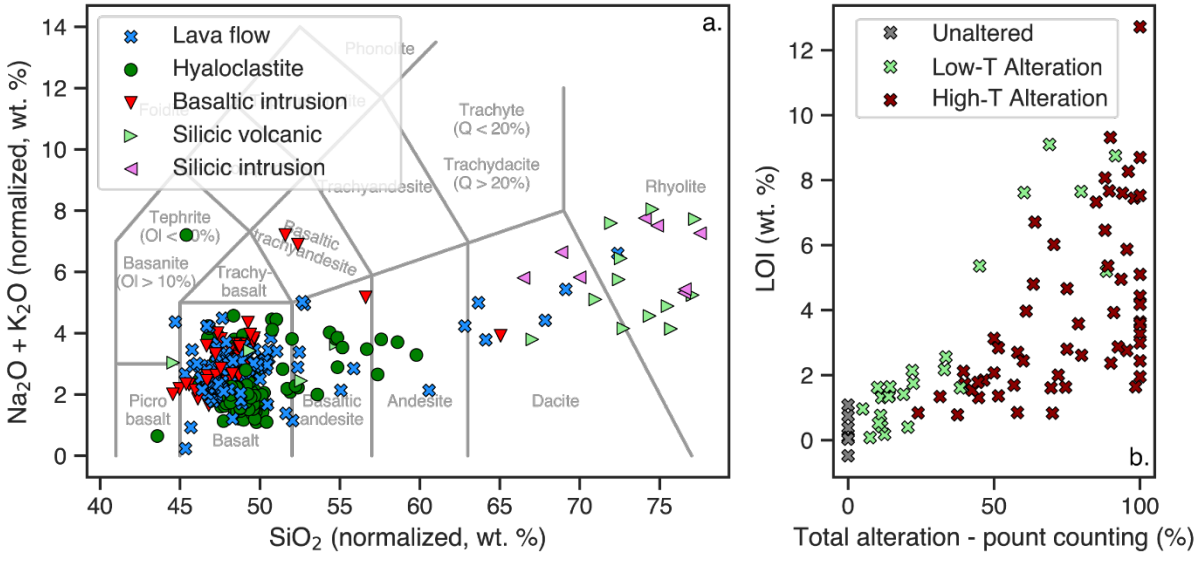

Figure 7. Whole-rock geochemical data and petrographic observations of alteration. a. Total alkali – silica (TAS) diagram (Le Maitre et al., 2002), with samples colored by lithology. Note that many of the rocks are very altered, and that sample lithologies are assigned based on the interpretation of the geological context and visual characteristics, rather than the geochemical field into which the rock plots. b. Loss on ignition (LOI) versus the total extent of alteration quantified by point counting. Only lava flows are shown, and symbols are colored by alteration – unaltered, low-T alteration (smectite-zeolite and mixed-layer clay zones), and high-T alteration (chlorite-epidote and epidote-amphibole zones).

https://doi.org/10.5194/essd-2022-279
Preprint. Discussion started: 17 August 2022

metric quantifying the extent alteration is loss on ignition (LOI), which was measured in many of the samples; while LOI is the sum of H_2O and CO_2, H_2O+, CO_2 and S_{total} were additionally separately analyzed in a subset of samples. Figure 7b shows the clear relationship between LOI and the extent of alteration quantified by point counting with LOI in a subset of lava flows, with the LOI increasing up to a maximum of ~12 wt. % as the degree of alteration approaches 100%.

The mineralogy of core samples from Lévy et al. (2018, 2019a, 2019b and 2020b) were analyzed using X-ray diffraction (XRD). Quantitative (crystalline) phase analysis was performed using Rietveld refinements of XRD patterns on randomly oriented mounts of whole rock powder samples. The powders were front-loaded onto the sample holder, using a razor blade to smoothen the surface and avoid preferred orientations (Bish et al., 1989). When several clay minerals with overlapping peaks (e.g. smectite and mixed layer smectite-chlorite) are present, Rietveld-refinements pose a problem of ambiguity for the quantitative analyses. Therefore, smectite quantification was performed by CEC measurements, after Lévy et al. (2020a) found a linear correlation between CEC and smectite content quantified using X-ray diffraction in samples where smectite is the only clay mineral.

The Cation Exchange Capacity (CEC) represents the total capacity of a rock medium to hold exchangeable cations, and is the sum of variable (pH-dependent) CEC and permanent CEC. While CEC in soil science is typically expressed in units of milli equivalent (meq), or mmol of electrons per 100 g rock, this is numerically equivalent to a given amount of charge per kg (1 meq 100 g^{-1} = 965.8 Coulomb kg^{-1}). To measure CEC on core samples from Krafla, Lévy et al. (2020a) modified a protocol originally designed to measure CEC on pure clay samples (Meir and Kahr, 1999) that uses Copper-triethyletetramine(II) 'Cu-trien'. The smectite content was then determined using the formula:

$$\frac{CEC}{CEC_0} = \frac{\rho_{dry}}{\rho_{smec}} \quad (11)$$

where ρ_{dry} and ρ_{smec} are the dry density of the sample and the density of smectite (in g/cm^3), respectively. The ratio $\frac{CEC}{CEC_0}$ is used as a measure of the smectite weight fraction, with CEC_0 = 91 meq/100 g the average CEC of pure smectite in these types of samples (Lévy et al. 2020a).

3.5 Other data: Acoustic velocities and mechanical properties

Acoustic velocities are available for relatively few samples in the database (Franzson and Tulinius, 1999; Frolova et al., 2005; Nono et al., 2020; Lévy et al., 2020b). Acoustic velocities express the propagation rate of mechanical waves – compressional P-waves and shear S-waves – in a bulk environment, composed of solid minerals and fluid in pores and fractures, either gas or liquid. While P-waves tend to travel faster in a water-saturated than dry environment, S-waves follow the reverse trend. For the samples from Lévy et al. (2020b), P- and S-wave velocities (V_p and V_s) were measured at a frequency of 500 kHz for both dry and wet samples, using a digital oscilloscope, a pulse generator and coupled piezoelectric transducers, at University of Montpellier. A coupling gel was used for V_p and honey for V_s. While the arrival time of P-waves is relatively easy to observe, that of S-waves arrival is often more ambiguous, yielding higher uncertainties. Figure 8 shows that P-wave velocities typically follow an inverse correlation to porosity: crystalline basalts show the highest velocities and the lowest porosities, while

https://doi.org/10.5194/essd-2022-279
Preprint. Discussion started: 17 August 2022

hyaloclastites have the lowest velocities and higher porosities. However, as P- and S-wave velocities are strongly dependent on crack density and geometry, low porosity but highly cracked rocks may display in some cases very low velocities at room conditions. This is observed for instance in S-wave velocities in low-porosity lava flows and intrusive rocks (Figure 8b).

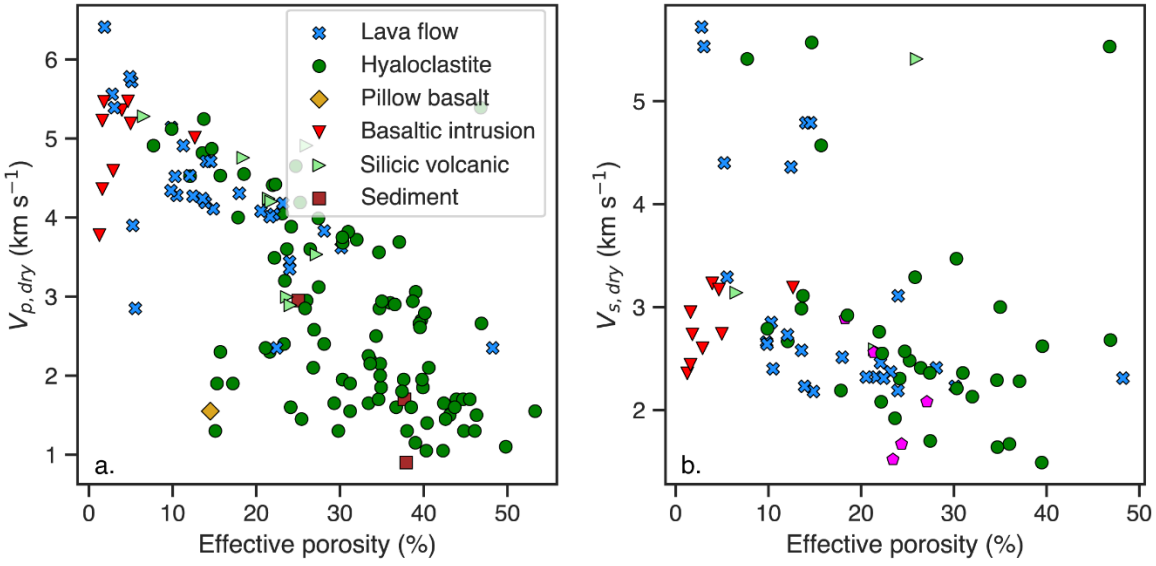

Figure 8. Acoustic velocities under dry (unsaturated) conditions versus effective porosity. Samples colored by lithology. a. P-wave velocities, b. S-wave velocities

Mechanical data (uniaxial compressive strength, Young's modulus, Poisson's ratio, and shear modulus) are available for even fewer samples (Frolova et al., 2005; Nono et al., 2020). Uniaxial compressive strength was measured on hyaloclastites in Frolova et al. (2005) using a German hydraulic press CDM-10/91.

4 Data availability

The database is archived at Zenodo at https://doi.org/10.5281/zenodo.6980232 (Scott et al., 2022) and is available under the Creative Commons Attribution 4.0 International license. This repository includes an Excel file containing separate worksheets, one listing sample metadata and petrophysical properties, a second listing geochemical and petrographic data, a third listing the file names of photographs corresponding to the sample IDs, a fourth listing additional hyaloclastite data (Frolova et al., 2005), and a fifth listing extended references. All worksheets are additionally included in the repository as csv files with the separator '|'. The photographs are also included in the Zenodo repository as a separate directory.

https://doi.org/10.5194/essd-2022-279
Preprint. Discussion started: 17 August 2022


Open Access Earth System Science Data Discussions

5 Concluding remarks & future status of the database

Icelandic rocks are generally of igneous or volcanic origin and mostly basaltic. The efforts of geologists over the past 50+ years has resulted in a tremendous amount of data, spanning petrophysical, geochemical, and petrographic measurements of a wide range of basaltic rocks and associated silicic and intermediate rocks in Iceland. However, it has historically been common that after publication of a paper or report, the only remaining manifestations of the data are the figures contained in the publication, and much of the raw underlying data is not accessible or difficult to access. This practice is only starting to change in response to the increasing emphasis on data availability. The motivation of the *Valgarður* database is to ensure that the results of decades of intensive study performed on Icelandic rocks remain accessible to future generations of geoscientists.

We hope that the availability of this database will also stimulate future research into the petrophysical properties of Icelandic rocks. Given the increasing emphasis on probabilistic (Bayesian) methods for geophysical inversions and numerical reservoir models, the data presented in this can be used to constrain the prior distributions assumed in geophysical inversions (Scott et al., 2019) and numerical models (e.g. Scott et al., 2022). The detailed sample descriptions, combined with the photographs of many of the sample sites included as a supplement to the dataset, should facilitate future research visits to the investigated areas. Moreover, the remaining cores from the Orkustofnun samples are now kept at Náttúrufræðistofnun (the Icelandic Institute of Natural History) for interested parties to continue research. There are clear gaps in the database, including the lack of samples from the central or northern parts of Iceland, as well as the lack of mechanical data. As future studies address these gaps in the data, we anticipate future releases of the database, and will use the versioning system available on Zenodo to make these updates available at the same repository given in this publication. Despite the gaps in the data, we believe that the present release of the *Valgarður* database will enhance the availability of this important data and provide a valuable resource for future studies investigating the interplay between the physical and chemical evolution of Icelandic rocks.

6 Sample availability

The remaining sample plugs from the Orkustofnun samples are now kept at Náttúrufræðistofnun (the Icelandic Institute of Natural History) and are available for future study.

7 Author contributions

Conceptualization: SWS, HF, LL, BG, JN, AV, MSG; Data curation: SWS, CC, LL, JF; Formal analysis: SS, HF, LL, BG; Funding acquisition: MSG, SWS; Methodology: HF, LL, CC; Resources: EJ, BG, HF, MSG, JN, AV; Writing – original draft preparation: SS, LL, BG, HF; Writing – review & editing: SS, LL, BG, HF, JF, MSG

https://doi.org/10.5194/essd-2022-279
Preprint. Discussion started: 17 August 2022

8 Competing interests

The authors declare that they have no conflict of interest.

9 Acknowledgements

SWS and CC received funding from the Technical Development Fund of the Research Center of Iceland (RANNÍS, grant number 175 193-0612 Data Fusion for Geothermal Reservoir Characterization). This project additionally received funding from Landsvirkjun Energy Research Fund (grant number NÝR-23-2019) We acknowledge Kristian Bär for sharing an early version of the P^3 PetroPhysical Property Database (Bär et al., 2020). The database represents the collective efforts of many scientists over many decades – we would like to gratefully acknowledge the contribution of everyone who helped in sample collection, measurement, and data management.

10 References

Adelinet M., Fortin, J., Guégin, Y., Schubnel, A. and Geoffroy, L.: Frequency and fluid effects on elastic properties of basalt: Experimental investigations, Geophys. Res. Lett., 37, L02303, https://doi.org/10.1029/2009GL041660, 2010.

Adelinet M., Fortin, J., Schubnel, A., and Guéguen, Y.: Deformation modes in an Icelandic basalt: From brittle failure to localized deformation bands. J. Volcanol. Geotherm. Res., 255, 15–25, https://doi.org/10.1016/j.jvolgeores.2013.01.011, 2013.

Aladejare, A. E. and Wang, Y.: Evaluation of rock property variability, Georisk Assess. Manag. Risk Eng. Syst. Geohazards, 11, 22–41, https://doi.org/10.1080/17499518.2016.1207784, 2017.

Anovitz, L. M. and Cole, D. R.: Characterization and analysis of porosity and pore structures, Rev. Mineral. Geochemistry, 80, 61–164, https://doi.org/10.2138/rmg.2015.80.04, 2015..

Arnórsson, S.: Geothermal systems in Iceland: Structure and conceptual models—I. High-temperature areas, 24, 561–602, 1995.

Asem, P. and Gardoni, P.: A generalized Bayesian approach for prediction of strength and elastic properties of rock, Eng. Geol., 289, 106187, https://doi.org/10.1016/j.enggeo.2021.106187, 2021.

Bär, K., Reinsch, T., and Bott, J.: The PetroPhysical Property Database (P3) – a global compilation of lab-measured rock properties. Earth Syst. Sci. Data, 12, 2485–2515, https://doi.org/10.5194/essd-12-2485-2020, 2020.

Bish, D. L., Reynolds, R. C., and Post, J. E.: Sample preparation for X-ray diffraction. In: eds. D. L. Bish and J. E. Post, Modern Powder Diffraction, Rev. Mineral. Geochemistry, 20, 73-99, 1989.

Browne P. R.: Hydrothermal Alteration in Active Geothermal Fields, Annu. Rev. Earth Planet. Sci., 6, 229–250, 1978.

Böðvarsson, G. and Walker, G.: Crustal Drift in Iceland, Geophys. J. R. Astron. Soc., 8, 285–300, 1964.

Burchardt, S. and Gudmundsson, A.: The infrastructure of Geitafell volcano, southeast Iceland, Stud. Volcanol. Leg. Georg. Walker, Spec. Publ. IAVCEI, 2, 349–370, 2009.

https://doi.org/10.5194/essd-2022-279
Preprint. Discussion started: 17 August 2022

485 Cant, J.L., Siratovich, P. A., Cole, J. W., Villeneuve, M. C., Kennedy, B. M. Matrix permeability of reservoir rocks, Ngatamariki geothermal field, Taupo Volcanic Zone, New Zealand, Geothermal Energy, 6, https://doi.org/10.1186/s40517-017-0088-6, 2018.

Ceryan, S., Tudes, S., and Ceryan, N.: A new quantitative weathering classification for igneous rocks, Environ. Geol., 55, 1319–1336, https://doi.org/10.1007/s00254-007-1080-4, 2008.

490 Colombier, M., Wadsworth, F. B., Gurioli, L., Scheu, B., Kueppers, U., Di Muro, A., and Dingwell, D. B.: The evolution of pore connectivity in volcanic rocks, Earth Planet. Sci. Lett., 462, 99–109, https://doi.org/ 10.1016/j.epsl.2017.01.011, 2017.

Cox, S. F.: Coupling between Deformation, Fluid Pressures, and Fluid Flow in Ore-Producing Hydrothermal Systems at Depth in the Crust, edited by:. J. W. Hedenquist, J. F. H. Thompson, R. J. Goldfarb, and J. P. Richards. SEG One Hundredth Anniv. Vol., 2005.

495 Dessert, C., Dupré, B., Gaillardet, J., François, L. M., Allègre, C. J.: Basalt weathering laws and the impact of basalt weathering on the global carbon cycle. Chem. Geol. 202, 257–273, https://doi.org/10.1016/j.chemgeo.2002.10.001, 2003.

Dobson, P. F., Kneafsey, T. J., Hulen J. and Simmons A.: Porosity, permeability, and fluid flow in the Yellowstone geothermal system, Wyoming, J. Volcanol. Geotherm. Res., 123, 313–324, 2003.

Eggertsson, G. H., Kendrick, J., Weaver, J., Wallace, P., Utley, J., Bedford, J., Allen, M., Markússon, S., Worden, R., Faulkner,

500 D. and Lavallée, Y.: Compaction of hyaloclastite from the active geothermal system at Krafla volcano, Iceland, Geofluids, 3878503, https://doi.org/10.1155/2020/3878503, 2020a.

Eggertsson, G. H., Lavallée, Y., Kendrick, J. E. and Markússon, S. H.: Improving fluid flow in geothermal reservoirs by thermal and mechanical stimulation: The case of Krafla volcano, Iceland, J. Volcanol. Geotherm. Res., 391, 106351, 2020b.

Escobedo, D.: Study of hydrothermal alteration and petrophysical properties of well KH6, Krafla geothermal field, NE Iceland,

505 Master's thesis, University of Montpellier, 2017.

Escobedo, D., Patrier, P., Beaufort, D., Gibert, B., Levy, L., Findling, N., and Mortensen, A.: Contribution of the paragenetic sequence of clay minerals to re-examination of the alteration zoning in the Krafla geothermal system, https://doi.org/ 10.3390/min11090935, 2021.

Filomena, C. M., Hornung, J., and Stollhofen, H.: Assessing accuracy of gas-driven permeability measurements: a comparative

510 study of diverse Hassler-cell and probe permeameter devices, Solid Earth, 5, 1–11, https://doi.org/10.5194/se-5-1-2014, 2014.

Flóvenz, Ó. G., Spangenberg, E., Kulenkampff, J., Árnason, K., Karlsdóttir, R. and Huenges, E.: The Role of Electrical Interface Conduction in Geothermal Exploration, in: Proceedings World Geothermal Congress, Antalya, Turkey, 24-29 April 2005, 2005.

Franzson, H.: Structure and petrochemistry of the Hafnarfjall-Skarðsheiði central volcano and the surrounding basalt

515 succession, W-Iceland, Ph.D. thesis, University of Edinburgh, 264 pp., 1978.

Franzson, H., Friðleifsson, G. O., Guðmundsson, A. and Vilmundardóttir, E. G.: Forðafræðistuðlar. Staðabergfræðirannsókna í lok 1997. (Reservoir Parameters. Status of petrological studies by the end of 1997). Orkustofnun, OS-97077, Reykjavik, Iceland, 1997.

https://doi.org/10.5194/essd-2022-279
Preprint. Discussion started: 17 August 2022

Franzson, H., and Tulinius, H.: Rannsóknir á kjarna úr holu ÖJ-1, Ölkelduhálsi (Research on core from hole ÖJ-1, Ölkelduháls), Orkustofnun (OS-99024), Reykjavik, Iceland, 1999.

Franzson, H., Guðlaugsson, S. Þ., and Friðleifsson, G. Ó.: Petrophysical properties of Icelandic rocks, in: Proceedings of the 6th Nordic Symposium on Petrophysics, Trondheim, Norway, 15-16 May 2001, 2001.

Franzson, H., Zierenberg, R. and Schiffman, P.: Chemical transport in geothermal systems in Iceland, J. Volcanol. Geotherm. Res., 173, 217–229, https://doi.org/ 10.1016/j.jvolgeores.2008.01.027, 2008.

Franzson, H., Guðfinnsson, G. and Helgadóttir, H.: Porosity, density and chemical composition relationships in altered Icelandic hyaloclastites, Water-Rock Interaction, edited by: Birkle and Torres-Alvarado. Taylor & Francis Group, London. pp. 199–202, 2010.

Franzson, H., Guðfinnsson, G. H., Frolova, J., Helgadóttir, H. M., Mortensen, A. K. and Jakobsson, S. P. Icelandic Hyaloclastite Tuffs. Iceland Geosurvey, ÍSOR-2011/064, 2011.

Franzson, H. and Gunnlaugsson, E.: Formation of clays and chlorites in the upper Icelandic crust, in: Proceedings World Geothermal Congress 2020+1, Reykjavik, Iceland, April-October 2021, 2020.

Friðleifsson, G.Ó.: Geology and alteration history of the Geitafell central volcano, Southeast Iceland, Ph.D. thesis, University of Edinburgh, 385 pp., 1983a.

Friðleifsson, G.Ó.: Mineralogical evolution of a hydrothermal system, in: Geothermal Resources Council Transactions, 7, 147–152, 1983b.

Friðleifsson, G.Ó.: Mineralogical evolution of a hydrothermal system. II. Heat sources-fluid interactions, in: Geothermal Resources Council Transactions, 8, 119-123, 1984.

Friðleifsson, I. B.: Petrology and structure of the Esja quaternary volcanic region, southwest Iceland, Ph.D. thesis, University of Oxford, 1973.

Friðleifsson, I. B.: Lithology and structure of geothermal reservoir rocks in Iceland. Orkustofnun, OSJHD-7531, Reykjavik, Iceland, 1975.

Friðleifsson, I. B.: Applied volcanology in geothermal exploration in Iceland, Pure Appl. Geophys. PAGEOPH, 117, 242–252, 1978.

Friðleifsson, G. Ó., and Vilmundardóttir, E. G.: Reservoir parameters TCP-project: A thin-section study of the Öskuhlíð samples. Orkustofnun, Reykjavik, Iceland, OS-98041, 1998.

Frolova, Y. V.: Patterns of transformations in the compositions and properties of Icelandic hyaloclastites during lithogenesis, Moscow Univ. Geol. Bull., 65, 104–114, https://doi.org/10.3103/s0145875210020067, 2010.

Frolova, J. V., Ladygin,, V. M., Franzson, H., Sigurðsson, O., Stefánsson, V. and Shustrov, V.: Petrophysical properties of fresh to mildly altered hyaloclastite tuffs, in: Proceedings World Geothermal Congress, Antalya, Turkey, 24-29 April 2005, 2005.

https://doi.org/10.5194/essd-2022-279
Preprint. Discussion started: 17 August 2022

Frolova, J., Ladygin, V., Rychagov, S., Zukhubaya, D. Effects of hydrothermal alterations on physical and mechanical properties of rocks in the Kuril-Kamchatka island arc, Eng. Geol. 183, 80–95, https://doi.org/10.1016/j.enggeo.2014.10.011, 2014.

Gibert, B., Loggia, D., Parat, F., Escobedo, D., Lévy, L., Friðleifsson, G.O., Pezard, P.A., Marino, N., Zierenberg, R.A., 2020. Petrophysical Properties of IDDP-2 Core Samples from Depths of 3650 to 4650m, in: Proceedings World Geothermal Congress 2020+1, Reykjavik, Iceland, April-October 2021, 2020.

Grab M., Zürcher, B., Maurer, H. and Greenhalgh, S. Seismic velocity structure of a fossilized Icelandic geothermal system: A combined laboratory and field study, Geothermics, 57, 84–94, https://doi.org/ 10.1016/j.geothermics.2015.06.004, 2015.

Guðmundsson, A., Franzson, H., and Friðleifsson, G. Ó. Forðafræðistuðlar. Söfnun sýna. (Reservoir parameters. Sample collection), Orkustofnun, Reykjavik, Iceland, OS-95017/JHD-11 B, 1995.

Harðardóttir, S., Matthews, S., Halldórsson, S. A., and Jackson, M. G.: Spatial distribution and geochemical characterization of Icelandic mantle end-members: Implications for plume geometry and melting processes, Chem. Geol., 120930, https://doi.org/ 10.1016/j.chemgeo.2022.120930, 2022.

Heap, M. J., Kennedy, B. M., Farquharson, J. I., Ashworth, J., Mayer, K., Letham-Brake, M., Reuschlé, T., Gilg, H. A., Scheu, B., Lavallée, Y., Siratovich, P., Cole, J., Jolly, A. D., Baud, P., and Dingwell, D. B.: A multidisciplinary approach to quantify the permeability of the Whakaari/White Island volcanic hydrothermal system (Taupo Volcanic Zone, New Zealand), J. Volcanol. Geotherm. Res., 332, 88–108, https://doi.org/ 10.1016/j.jvolgeores.2016.12.004, 2017.

Heap, M. J., Gravley, D. M., Kennedy, B. M., Gilg, H. A., Bertolett, E., and Barker, S.L.L.: Quantifying the role of hydrothermal alteration in creating geothermal and epithermal mineral resources: The Ohakuri ignimbrite (Taupō Volcanic Zone, New Zealand). J. Volcanol. Geotherm. Res. 390, 106703. https://doi.org/10.1016/j.jvolgeores.2019.106703, 2020.

Heap, M. J. and Violay, M. E. S.: The mechanical behaviour and failure modes of volcanic rocks: a review, Bull. Volcanol., 83, https://doi.org/10.1007/s00445-021-01447-2, 2021.

Heap, M.J., Harnett, C.E., Wadsworth, F.B., Gilg, H.A., Carbillet, L., Rosas-Carbajal, M., Komorowski, J.C., Baud, P., Troll, V.R., Deegan, F.M., Holohan, E.P., Moretti, R.: The tensile strength of hydrothermally altered volcanic rocks. J. Volcanol. Geotherm. Res. 428, 107576, https://doi.org/10.1016/j.jvolgeores.2022.107576, 2022.

Jaya, M. S., Shapiro, S. A., Kristinsdóttir, L. H., Bruhn, D., Milsch, H., and Spangenberg, E.: Temperature dependence of seismic properties in geothermal rocks at reservoir conditions, Geothermics, 39, 115–123, https://doi.org/ 10.1016/j.geothermics.2009.12.002, 2010.

Klinkenberg, L. J.: The permeability of porous media to liquids and gases. In *Drilling and production practice*, 1941

Kristinsdóttir, L. H., Flóvenz, Ó. G., Árnason, K., Bruhn, D., Milsch, H., Spangenberg, E., and Kulenkampff, J.: Electrical conductivity and P-wave velocity in rock samples from high-temperature Icelandic geothermal fields, 39, 94–105, https://doi.org/10.1016/j.geothermics.2009.12.001, 2010.

Kristmannsdottir, H., & Tomasson, J.: Zeolite zones in geothermal areas in Iceland. Orkustofnun, Reykjavik, Iceland, OS-JHD-7649, 1978.

https://doi.org/10.5194/essd-2022-279
Preprint. Discussion started: 17 August 2022

585 Kristmannsdóttir, H.: Alteration of basaltic rocks by hydrothermal activity at 100-300C, Dev. Sedimentol., 27, 359–367, 1979.

Kummerow, J., Raab, S., Schuessler, J. A., and Meyer, R.: Non-reactive and reactive experiments to determine the electrical conductivities of aqueous geothermal solutions up to supercritical conditions, J. Volcanol. Geotherm. Res., 391, 106388, doi.org/10.1016/j.jvolgeores.2018.05.014, 2020.

Le Maitre, R., Streckeisen, A., Zanettin, B., Le Bas, M., Bonin, B., & Bateman, P.: Igneous Rocks: A classification and glossary
590 of terms: Recommendations of the international union of geological sciences subcommission on the systematics of igneous rocks (2nd ed.). Cambridge, Cambridge University Press. https://doi.org/10.1017/CBO9780511535581, 2002:

Lévy, L., Gibert, B., Sigmundsson, F., Flóvenz, O. G., Hersir, G. P., Briole, P., and Pezard, P. A.: The role of smectites in the electrical conductivity of active hydrothermal systems: Electrical properties of core samples from Krafla volcano, Iceland, Geophys. J. Int., 215, 1558–1582, https://doi.org/10.1093/gji/ggy342, 2018.

595 Lévy, L., Gibert, B., Sigmundsson, F., Deldicque, D., Parat, F., and Hersir, G. P.: Tracking Magmatic Hydrogen Sulfur Circulations Using Electrical Impedance: Complex Electrical Properties of Core Samples at the Krafla Volcano, Iceland, J. Geophys. Res. Solid Earth, 124, 2492–2509, https://doi.org/10.1029/2018JB016814, 2019a.

Lévy, L., Weller, A., and Gibert, B.: Influence of smectite and salinity on the imaginary and surface conductivity of volcanic rocks, Near Surf. Geophys., 17, 653–673, https://doi.org/10.1002/nsg.12069, 2019b.

600 Lévy, L., Friðriksson, T., Findling, N., Lanson, B., Fraisse, B., Marino, N., and Gibert, B.: Smectite quantification in hydrothermally altered volcanic rocks, 85, 101748, https://doi.org/ 10.1016/j.geothermics.2019.101748, 2020.

Lévy, L. E., Gibert, B., Escobedo, D., Patrier, P., Lanson, B., Beaufort, D., Loggia, D., Pezard, P. A., and Marino, N.: Relationships between lithology, permeability, clay mineralogy and electrical conductivity in Icelandic altered volcanic rocks, in: Proceedings World Geothermal Congress 2020+1, Reykjavik, Iceland, April-October, 2020, 2020.

605 Liotta, D., Brogi, A., Ruggieri, G., Rimondi, V., Zucchi, M., Helgadóttir, H. M., Montegrossi, G., and Friðleifsson, G. Ó.: Fracture analysis, hydrothermal mineralization and fluid pathways in the Neogene Geitafell central volcano: insights for the Krafla active geothermal system, Iceland, J. Volcanol. Geotherm. Res., 391, 106502, https://doi.org/ 10.1016/j.jvolgeores.2018.11.023, 2020.

Lonker, S. W., Franzson, H., and Kristmannsdöttir, H.: Mineral-fluid interactions in the Reykjanes and Svartsengi geothermal
610 systems, Iceland, Am. J. Sci., 293, 605–670, 1993.

Milsch, H., Kristinsdóttir, L. H., Spangenberg, E., Bruhn, D., and Flóvenz, Ó. G.: Effect of the water-steam phase transition of the electrical conductivity of porous rocks, 39, 106–114, https://doi.org/ 10.1016/j.geothermics.2009.09.001, 2010.

Mordensky, S. P., Villeneuve, M. C., Kennedy, B. M., Heap, M. J., Gravley, D. M., Farquharson, J. I., and Reuschlé, T.: Physical and mechanical property relationships of a shallow intrusion and volcanic host rock, Pinnacle Ridge, Mt. Ruapehu,
615 New Zealand, J. Volcanol. Geotherm. Res., 359, 1–20, https://doi.org/ 10.1016/j.jvolgeores.2018.05.020, 2018.

Navelot, V., Géraud, Y., Favier, A., Diraison, M., Corsini, M., Lardeaux, J.M., Verati, C., Mercier de Lépinay, J., Legendre, L., Beauchamps, G., 2018. Petrophysical properties of volcanic rocks and impacts of hydrothermal alteration in the Guadeloupe Archipelago (West Indies). J. Volcanol. Geotherm. Res. 360, 1–21, https://doi.org/10.1016/j.jvolgeores.2018.07.004, 2018.

https://doi.org/10.5194/essd-2022-279
Preprint. Discussion started: 17 August 2022

Nicolas, A., Lévy, L., Sissmann, O., Li, Z., Fortin, J., Gibert, B., Sigmundsson, F.: Influence of hydrothermal alteration on the elastic behaviour and failure of heat-treated andesite from Guadeloupe, Geophys. J. Int. 223, 2038–2053, https://doi.org/10.1093/gji/ggaa437, 2020.

Nono, F., Gibert, B., Parat, F., Loggia, D., Cichy, S. B., and Violay, M.: Electrical conductivity of Icelandic deep geothermal reservoirs up to supercritical conditions: Insight from laboratory experiments, J. Volcanol. Geotherm. Res., 391, 106364, https://doi.org/ 10.1016/j.jvolgeores.2018.04.021, 2020.

Orkustofnun: https://orkustofnun.is/orkustofnun/frettir/valgardur-gagnagrunnur-fordafraedistudla-gerdur-adgengilegur, last access 21.7.2022, 2018

Pálmason, G.: A continuum model of crustal generation in Iceland-kinematic aspects, Journal of Geophysics, 47, 1, 7-18, 1980.

Pálsson, S.: Mælingar á eðlisþyngd og poruhluta bergs (Measurements of the density and porosity of rock), Orkustofnun, Reykjavik, Iceland, 1972.

Pálsson, S., Haraldsson, G. I., and Vigfússon, G. H.: Eðlismassi og poruhluti bergs (Density and Porosity of Rock), Orkustofnun, Reykjavik, Iceland, 35 pp., OS-84048, 1984.

Petford, N.: Controls on primary porosity and permeability development in igneous rocks, Geol. Soc. London, Spec. Publ., 214, 93 LP – 107, https://doi.org/10.1144/GSL.SP.2003.214.01.06, 2003.

Pola, A., Crosta, G., Fusi, N., Barberini, V., and Norini, G.: Influence of alteration on physical properties of volcanic rocks, 566–567, 67–86, https://doi.org/ 10.1016/j.tecto.2012.07.017, 2012.

Pola, A., Crosta, G. B., Fusi, N., and Castellanza, R.: General characterization of the mechanical behaviour of different volcanic rocks with respect to alteration, Eng. Geol., 169, 1–13, https://doi.org/ 10.1016/j.enggeo.2013.11.011, 2014.

Rink, M., and Schopper, J. R.: Interface conductivity and its implications to electric logging, in: SPWLA 15th Annual Logging Symposium. McAllen, Texas, June 1974, SPWLA-1974-J, 1974.

Sanchez-Alfaro, P., Reich, M., Arancibia, G., Pérez-Flores, P., Cembrano, J., Driesner, T., Lizama, M., Rowland, J., Morata, D., Heinrich, C. A., Tardani, D., and Campos, E.: Physical, chemical and mineralogical evolution of the Tolhuaca geothermal system, southern Andes, Chile: Insights into the interplay between hydrothermal alteration and brittle deformation, J. Volcanol. Geotherm. Res., 324, 88–104, https://doi.org/10.1016/j.jvolgeores.2016.05.009, 2016.

Saripalli, K. P., Meyer, P. D., Bacon, D. H., and Freedman, V. L.: Changes in Hydrologic Properties of Aquifer Media Due to Chemical Reactions: A Review, Crit. Rev. Environ. Sci. Technol., 31, 311–349, https://doi.org/10.1080/20016491089244, 2001.

Scott, S. W., Covell, C., Júlíusson, E., Valfells, Á., Newson, J., Hrafnkelsson, B., Gudjónsdóttir, M. S.: A probabilistic geologic model of the Krafla geothermal system constrained by gravimetric data, Geotherm. Energy, 7, https://doi.org/10.1186/s40517-019-0143-6, 2019.

Scott, S. W., O'Sullivan, J. P., Maclaren, O. J., Nicholson, R., Covell, C., Newson, J., Guðjónsdóttir, M. S.: Bayesian Calibration of a Natural State Geothermal Reservoir Model, Krafla, North Iceland, Water Resour. Res., 58, https://doi.org/10.1029/2021wr031254, 2022.

https://doi.org/10.5194/essd-2022-279
Preprint. Discussion started: 17 August 2022

Scott, Samuel W., Lévy, Léa, Covell, Cari, Franzson, Hjalti, Gibert, Benoit, Valfells, Ágúst, Newson, Juliet, Frolova, Julia, & Guðjónsdóttir, María Sigríður: Valgarður: A Database of the Petrophysical, Mineralogical, and Chemical Properties of Icelandic Rocks (1.0) [data set], https://doi.org/10.5281/zenodo.6980232, 2022.

Schön, J. H. : Physical Properties of Rocks, vol. 65, Elsevier, ii, https://doi.org/ 10.1016/B978-0-08-100404-3.09990-X, 2015.

Sigmarsson, O. and Steinthórsson, S.: Origin of Icelandic basalts: A review of their petrology and geochemistry, J. Geodyn., 43, 87–100, https://doi.org/10.1016/j.jog.2006.09.016, 2007.

Sigmarsson, O., Maclennan, J., and Carpentier, M.: Geochemistry of igneous rocks in Iceland: a review. Jökull, 58, 139-160, 2008.

Sigurðsson Ó. and Stefánsson V.: Forðafræðistuðlar. Mælingar á bergsýnum. (Reservoir parameters. Measurements on rock samples, Orkustofnun, Reykjavik, Iceland, OS-94049/JHD-28B, 1994.

Sigurðsson Ó.: Forðafræðistuðlar. Reynslusamband til að breyta mældri gaslekt í vatnslekt. (Reservoir parameters. An empirical relationship to change measured gas permeability to water permeability), Orkustofnun, Reykjavik, Iceland, (OS-98065, 1998a.

Sigurðsson Ó., Forðafræðistuðlar. Lekt og hárpípulíkan (Reservoir parameters. Permeability and capillary tube model), Orkustofnun, Reykjavik, Iceland, OMAR-1998/01, 1998b.

Sigurðsson, Ó., Guðmundsson, Á., Friðleifsson, G. Ó., Franzson, H., Guðlaugsson, S. Þ., and Stefánsson, V.: Database on igneous rock properties in Icelandic geothermal systems. Status and unexpected results. In: Proceedings World Geothermal Congress 2000, Kyushu – Tohoku, Japan, May 28-June 10, 2000, 2881–2886, 2000.

Sigurðsson, Ó. and Stefánsson, V.: Porosity structure of Icelandic basalt, Proc. Est. Acad. Sci. Geol., 51, 33–46, https://doi.org/10.3176/geol.2002.1.03, 2002.

Snæbjörnsdóttir, S., Sigfússon, B., Marieni, C., Goldberg, D., Gislason, S. R., and Oelkers, E. H.: Carbon dioxide storage through mineral carbonation, https://doi.org/10.1038/s43017-019-0011-8, 2020.

Stefánsson, V., Sigurðsson, O., Guðmundsson, Á., Franzson, H., Friðleifsson, G. Ó., and Tulinius, H.: Core Measurements and Geothermal Modelling, in: Second Nordic Symposium on Petrophysics: Fractured reservoirs, edited by: M. F. Middleton, 198-220, 1997.

Stroncik, N. A. and Schmincke, H. U.: Palagonite - A review, Int. J. Earth Sci., 91, 680–697, https://doi.org/10.1007/s00531-001-0238-7, 2002.

Sveinbjörnsdóttir, Á.: Composition of geothermal minerals from saline and dilute fluids—Krafla and Reykjanes, Iceland, 27, 301–315, 1992.

Thien, B. M. J., Kosakowski, G., and Kulik, D. A.: Differential alteration of basaltic lava flows and hyaloclastites in Icelandic hydrothermal systems, 3, 11, https://doi.org/10.1186/s40517-015-0031-7, 2015.

Thompson, A. B.: Flow and focusing of metamorphic fluids, in: Fluid Flow and Transport in Rocks, edited by: Jamtveit, B., 297-314, 1997.

https://doi.org/10.5194/essd-2022-279
Preprint. Discussion started: 17 August 2022

Villeneuve, M. Kennedy, B., Gravley, D., Mordensky, S., Heap, M. J., Siratovich, P., Wyering, L., and Cant, J.: Characteristics of altered volcanic rocks in geothermal reservoirs, in: da Fontoura, S.A.B., Rocca, R.J., & Mendoza, J.F.P. (Eds.). Rock Mechanics for Natural Resources and Infrastructure Development, CRC Press. https://doi.org/10.1201/9780367823177, 2019.

Vinciguerra, S., Trovato, C., Meredith, P. G., and Benson, P. M.: Relating seismic velocities, thermal cracking and permeability in Mt. Etna and Iceland basalts, Int. J. Rock Mech. Min. Sci., 42, 900–910, https://doi.org/10.1016/j.ijrmms.2005.05.022, 2005.

Walker, G. P. L.: Zeolite zones and dike distribution in relation to the structure of the basalts of eastern Iceland, J. Geol., 68, 515–528, 1960.

Walker, G. P. L.: The Breiddalur central volcano, eastern Iceland, Q. J. Geol. Soc., 119, 29–63, https://doi.org/10.1144/gsjgs.119.1.0029, 1963.

Walker, G. P. L.: Eruptive Mechanisms in Iceland. Geodynamics of Iceland and the North Atlantic Area, edited by: Kristjansson, L., Springer Netherlands, Dordrecht, 189–201, 1974.

Waxman, M. H., Smits, L. J. M: Electrical conductivities in oil-bearing shaly sands, Soc. Pet. Eng. J., 8, 107–122, 1968.

Weaver, J., Eggertsson, G. H., Utley, J. E. P., Wallace, P. A., Lamur, A., Kendrick, J. E., Tuffen, H., Markússon, S. H., and Lavallée, Y.: Thermal liability of hyaloclastite in the Krafla geothermal reservoir, Iceland: The impact of phyllosilicates on permeability and rock strength, https://doi.org/10.1155/2020/9057193, 9057193, 2020.

Weydt, L. M., Ramírez-Guzmán, Á. A., Pola, A., Lepillier, B., Kummerow, J., Mandrone, G., Comina, C., Deb, P., Norini, G., Gonzalez-Partida, E., Ramón Avellán, D., Maciás, J. L., Bär, K., and Sass, I.: Petrophysical and mechanical rock property database of the Los Humeros and Acoculco geothermal fields (Mexico), Earth Syst. Sci. Data, 13, 571–598, https://doi.org/10.5194/essd-13-571-2021, 2021.

Wolff-Boenisch, D., Gislason, S.R., Oelkers, E.H.: The effect of crystallinity on dissolution rates and CO2 consumption capacity of silicates, Geochim. Cosmochim. Acta 70, 858–870, https://doi.org/10.1016/j.gca.2005.10.016, 2006.

Wyering, L. D., Villeneuve, M. C., Wallis, I. C., Siratovich, P. A., Kennedy, B. M., Gravley, D. M., and Cant, J. L.: Mechanical and physical properties of hydrothermally altered rocks, Taupo Volcanic Zone, New Zealand, J. Volcanol. Geotherm. Res., 288, 76–93, https://doi.org/10.1016/j.jvolgeores.2014.10.008, 2014.